Structural and Magnetic Properties of MBE Grown (Fe/Pt) (111) Multilayers

A. Marynowska[a], E. Dynowska[a], S. Lewińska[a], T. Seki[b], K. Takanashi[b], J. Kanak[c], A. Pietruczik[a], P. Aleszkiewicz[a], A. Wawro[a], A. Ślawska-Waniewska[a] and L.T. Baczewski[a,*]

[a]Institute of Physics, Polish Academy of Sciences, Aleja Lotnikow 32/46, PL–02668 Warsaw, Poland
[b]Institute for Materials Research, Sendai, Japan
[c]AGH University of Science and Technology, Cracow, Poland

(Received September 8, 2016; in final form October 18, 2016)

Series of $Al_2O_3(0001)/Pt/(Fe/Pt)_n/Pt$ multilayers with variable number of bilayers n and thicknesses of individual layers were grown using molecular beam epitaxy to investigate influence of buffer layer structure, number of bilayers, and individual layer thickness on their structural and magnetic properties. Both columnar and monocrystalline 10 nm Pt (111) buffer layers were used in the experiment. Structure of Pt buffer layer determined the roughness of Fe/Pt interfaces and consequently magnetic properties of the multilayers. When multilayers were deposited on columnar Pt buffer layer, we observed increase of Fe/Pt interfaces roughness with increasing number of bilayers to values exceeding the nominal Fe/Pt bilayer thickness in the upper part of the sample volume, which resulted in the increment of coercivity in the sample with $n = 15$ determined from hysteresis loops measured for perpendicular orientation of magnetic field. When Fe/Pt multilayers were deposited on monocrystalline Pt buffer layer, Fe/Pt interfaces were smooth regardless the number of bilayers. All samples, despite of the quality of buffer layer, number of bilayers, and individual layer thickness revealed easy magnetisation axis oriented in the sample plane.

DOI: 10.12693/APhysPolA.130.1363

PACS/topics: 61.05.cp, 61.05.jh, 68.35.bd, 68.35.Ct, 68.37.Ef, 68.37.Ps, 68.65.Ac, 75.50.Bb, 75.70.Ak

1. Introduction

FePt $L1$ films have recently attracted a lot of attention because of possible applications as rare-earth free perpendicular high density recording media. Large perpendicular magnetic anisotropy with K_u constant up to 7×10^7 erg/cm^3 [1] is correlated with CuAu-I type chemical ordering in FePt $L1$ alloys. Such alloys are mostly fabricated by post growth annealing of multilayers or disordered alloys but none of these methods allows patterning of easy magnetisation direction on nano- or microscale. To make it possible it is crucial to first obtain reliable and reproducible procedure of fabrication of Fe/Pt multilayers with in-plane easy magnetisation which could be further locally modified (e.g. by irradiation through a shadowing masks [2] or by focused ion beam irradiation [3]) in order to change its structure to fct which is characteristic for $L1_0$-type alloy, resulting in switching of easy magnetisation direction into perpendicular direction in the modified sample volume.

In this paper we report a detailed study of structural and magnetic properties of (111) Fe/Pt multilayers depending on buffer layer crystalline structure, number of bilayers, and individual layer thickness. Presented data can be a starting point both for creating patterned media by local modification of multilayers [2, 3] or for creating tilted magnetic recording media [4]. Most attention in the literature is being focused on Fe/Pt multilayers and alloys oriented in (001) direction. From the data storage point of view, a substantial disadvantage of $L1$-ordered films oriented in (001) direction is that high magnetic field is required to switch magnetisation direction during the data writing process. Therefore (111)-oriented FePt systems have been investigated lately [5–8] due to the features important from the technological point of view. Firstly the (111) plane is the close-packed one so thin FePt film can be deposited on amorphous substrates on which they grow having (111) texture and after annealing $L1_0$ phase can be obtained [5, 9]. Secondly, (111)-oriented $L1_0$-ordered FePt films can be used in tilted perpendicular recording as its easy magnetisation axis is counted 34° from the film plane resulting in lowering by up to 50% of the required normalized switching field [10, 11]. Although some information on Fe/Pt (111) multilayers structure and their magnetic properties can be found in the literature [12–17], a study of influence of thin film sample structure on magnetic properties in Fe/Pt multilayers deposited on monocrystalline substrate in relation to buffer layer crystalline structure and number of layers has not been reported so far.

2. Experimental details

2.1. Experimental techniques

Two series of samples were prepared using molecular beam epitaxy (MBE) technique Al_2O_3 (0001)/Pt 10 nm/(Fe 0.5 nm/Pt 0.3 nm)$_n$

*corresponding author; e-mail: bacze@ifpan.edu.pl

/Pt 5 nm (n = 5, 10, 15) multilayers fabricated on Pt buffer layer with columnar growth mode and Al_2O_3 (0001)/Pt 10 nm/(Fe X nm/Pt X nm)$_n$/Pt 10 nm (n = 5, 10, 15; X = 0.5 or 1 nm) multilayers grown on monocrystalline Pt buffer layer. Deposition rate was measured with precalibrated quartz microbalance. Base pressure in MBE deposition chamber was 10^{-10} Torr. Substrate holder was rotated during deposition with the frequency of 42°/s. Pt was deposited using e-gun with the deposition rate of 0.03 nm/s and Fe — from the Knudsen cell with the rate 0.01 nm/s. Pt buffer layers were deposited at various conditions listed in Table I Fe/Pt multilayers and Pt cover layers were deposited at room temperature.

Structural properties of the samples were investigated by *in situ* reflection high energy electron diffraction (RHEED), low energy electron diffraction (LEED) and scanning tunnelling microscopy (STM) and *ex situ* using atomic force microscopy (AFM) in a tapping mode, X-ray reflectometry (XRR), and X-ray diffractometry (XRD). The XRD measurements were performed using PANalytical Empyrean X-ray diffractometer with Cu K_{α_1} radiation, equipped with the Johansson monochromator Ge(111) in the incident beam and a linear semiconductor strip detector.

$M(H)$ hysteresis loops of the Fe/Pt multilayers were investigated *ex situ* using magneto-optic Kerr effect (MOKE) magnetometer and vibrating sample magnetometer (VSM).

2.2. Substrate preparation and sample growth

In our experiment Al_2O_3 (0001) oriented substrates were used to promote formation of Pt fcc (111) buffer layer structure [18–22] and further (111) orientation of successive Fe/Pt bilayers. (0001) Al_2O_3 surface morphology is well known to strongly depend on preparation procedure e.g. cleaning methods, annealing time [23, 24] and temperature [23–26], and atmosphere [27]. Al_2O_3 (0001) substrates were cleaned using two different methods. *Method 1* consisted of subsequent cleaning of Al_2O_3 in acetone, methanol, deionised water, mixture of ultrapure water with H_2O_2 and H_2SO_4 in 2:1:1 ratio at room temperature, and again in deionised water. In *method 2* a different etching solution was used: the mixture of H_2O_2, NH_4OH and ultrapure water in 1:1:5 ratio at 70–80 °C.

TABLE I

Comparison of Al_2O_3 substrate and 10 nm Pt buffer layers A–E preparation procedures and basic conclusions on the buffer layer structure obtained from RHEED and AFM images. RT — room temperature.

Buffer layer	A	B	C	D	E
Al_2O_3 cleaning	method 1	method 1	method 1	method 1	method 2
Al_2O_3 pre-annealing	–	1200 °C/30 min	1200 °C/30 min	1200 °C/30 min	1200 °C/30 min
Pt deposition temperature	RT	640 °C	RT	RT	750 °C
Pt post-annealing	–	–	–	640 °C/15 min	–
Pt structure (from RHEED images)	polycrystalline	columnar	polycrystalline	columnar	monocrystalline
Pt surface (from AFM images)	regular steps	granular surface	regular steps	granular surface	granular surface
RMS roughness (from AFM images)	0.280 nm	0350 nm	0190 nm	0195 nm	0174 nm

Pt film structure and its surface roughness are also extremely sensitive to heat treatment and even small deviations from specific temperature may result in different growth mode. As it was reported before [18–20] by manipulating the substrate temperature during deposition or post-annealing time and temperature one may engineer Pt films of different structure. Due to significant dependence of Pt morphology on growth conditions we performed a detailed study to determine optimal conditions for epitaxial growth of 10 nm Pt (111) buffer layer on Al_2O_3 (0001). It was essential to further achieve multilayer samples of small interface roughness and to

compare structural and magnetic properties of multilayers deposited on different buffer layers. Different substrate cleaning methods and various growth conditions were used. Four buffer layers denoted as A, B, C and D were prepared on substrates cleaned with method 1 and buffer layer E was deposited on a substrate prepared using method 2. All the substrate and Pt buffer layer details are listed in Table I.

3. Results and discussion

3.1. Pt buffer layer

AFM images showing the surface morphology of Pt buffer layers deposited at room temperature (Fig. 1A,C,D) and at 640 °C (Fig. 1B) are presented in Fig. 1. Pt grains size is visibly larger for deposition temperature of 640 °C (Fig. 1B) and for Pt buffer annealed at this temperature after growth (see Fig. 1D). Obvious similarities were also observed in RHEED images: rings indicating a presence of polycrystalline films were visible when buffer layers were deposited at RT (buffer layers A and C) regardless of the type of a substrate heat treatment. Deposition at 640 °C (buffer layer B) allowed to obtain disordered columnar structure. By disordered columnar structure we mean grains well-oriented in the direction perpendicular to the film surface but disordered in the azimuthal orientation resulting in sharp streaks in RHEED images but with their positions independent of the sample angle with respect to the electron beam direction. Post-growth annealing at 640 °C after RT deposition of Pt (buffer layer D) revealed even sharper streaks in RHEED images arising from smoothening of the Pt surface but still of columnar structure.

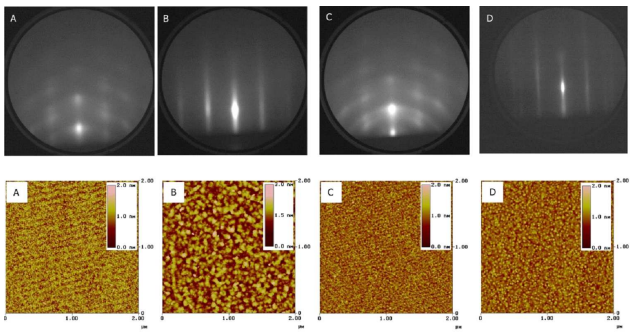

Fig. 1. AFM and RHEED images of buffer layers A–D. For all buffer layers AFM picture size is 2 µm × 2 µm and colour scale is 0–2 nm. RHEED images of all presented buffer layers (A–D) were independent of the sample angular position with respect to the electron beam.

Considering absence of monocrystalline structure of Pt buffer layers A–D deposited on sapphire substrates prepared by method 1, another attempt to obtain monocrystalline smooth Pt buffer layer was made using substrate cleaned by method 2. This procedure of Al_2O_3 substrate cleaning, together with substrate pre-annealing and Pt deposition at 750 °C allowed us to obtain monocrystalline (111) Pt layer (buffer layer E) confirmed by *in situ* RHEED, LEED, STM, and *ex situ* AFM measurements presented in Fig. 2.

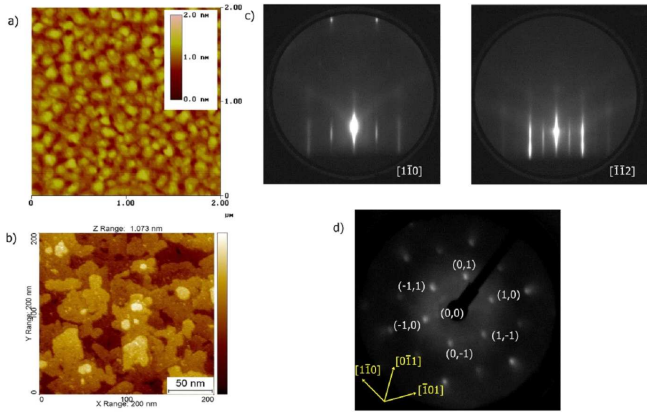

Fig. 2. Surface structure of 10 nm Pt buffer layer E: (a) AFM image — picture size is 2 µm × 2 µm and colour scale is 0–2 nm, (b) STM image — picture size is 200 nm × 200 nm and Z range is 1073 nm, (c) RHEED images, (d) LEED image.

It is well known [18–22] that the sixfold symmetry of the (0001) Al_2O_3 surface induces the (111) orientation of fcc sixfold platinum symmetry which can be seen in RHEED and LEED images. In RHEED images of buffer E (Fig. 2), in contrast to buffer layers A–D, streaks positions were dependent of the sample angular orientation against the electron beam direction which — together with AFM images — indicate that Pt buffer layer is monocrystalline with low roughness and grows in (111) direction RMS roughness of buffer layer E calculated from AFM image is 0174 nm which is the lowest value among all the investigated buffer layers (A–E). More details of the Pt surface structure were revealed by *in situ* STM measurement: Pt during growth creates flat and wide (10–80 nm) monoatomic-height terraces.

For further studies of the Pt buffer layer structure influence on magnetic and structural properties of Fe/Pt multilayers two buffer layers were chosen from all described above: buffer layer D of disordered columnar structure and monocrystalline buffer layer E. Buffer layer D was chosen as it has the lowest RMS roughness value among all Pt buffer layers with columnar structure.

3.2. Structural properties of Fe/Pt multilayers deposited on columnar Pt 10 nm buffer layer (D)

Multilayers of Al_2O_3 (0001)/Pt 10 nm/(Fe 0.5 nm/Pt 0.3 nm)$_{15}$/Pt 5 nm configuration were deposited on the buffer layer of disordered columnar structure (buffer layer D). RHEED investigations performed during growth on each successive layer revealed important information (Fig. 3a). Continuation of columnar growth was observed for successive Fe/Pt multilayers (RHEED patterns independent of the crystal orientation against the electron beam direction), which is the same growth mode as for the Pt buffer layer D. On the

other hand, during growth of successive Fe and Pt layers we observed RHEED intensity oscillations suggesting 2D growth mode RHEED images also revealed some roughening of the Fe/Pt interface with increasing number of bilayers (streaks broadening and occurrence of dilated spots).

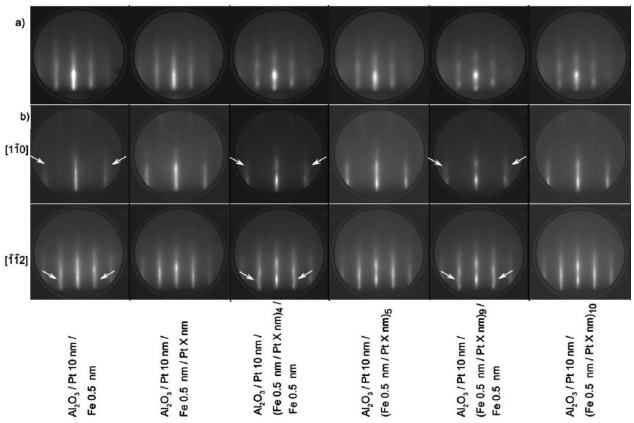

Fig. 3. RHEED investigations of consequent Fe and Pt layers structure in Fe/Pt multilayers as a function of number of bilayers. Row (a) — RHEED images of selected layers of the Fe/Pt multilayer sample prepared on the columnar buffer layer D (RHEED image is independent of sample angular position with respect to e-beam direction), row (b) — RHEED images of corresponding Fe and Pt layers of the multilayer sample prepared on the monocrystalline buffer layer E for two different directions of the incident electron beam; the arrows show splitting of the streaks on Fe layers. Pt layer thickness in multilayers: $X = 0.3$ nm (row (a)) and $X = 0.5$ nm (row (b)).

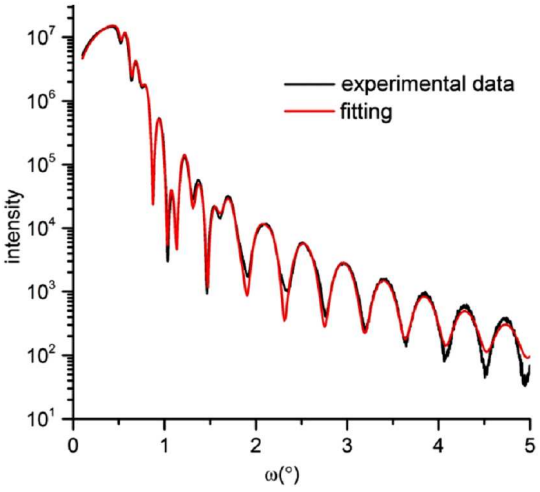

Fig. 4. XRR pattern of the sample of $Al_2O_3(0001)$/ Pt 10 nm/(Fe 0.5 nm/Pt 0.3 nm)$_{15}$/Pt 5 nm deposited on the columnar Pt buffer layer (D) together with fitting of the theoretical pattern.

To investigate quantitatively how the interface roughness changes with the increasing number of bilayers, X-ray reflectivity (XRR) measurement was performed. Roughness of the Al_2O_3 surface was only 0.6 nm. Pt buffer layer D thickness calculated from XRR measurement was 98 nm which is in a good agreement with the nominal thickness of 10 nm, and its surface roughness was 0.22 nm (RMS roughness calculated from AFM image was 0.174 nm). XRR pattern simulation shown in Fig. 4 suggests that roughness of subsequent Fe/Pt interfaces increases with increasing number of bilayers and reaches up to 0.9 nm in the topmost part of the sample consisting of 15 bilayers. Only with this assumption fitting of the experimental data was possible. This value exceeds the nominal Fe/Pt bilayer thickness, which is 0.8 nm which means formation of the region with higher Fe/Pt interface roughness in the upper part of the sample, between 11th and 15th bilayer.

Influence of bilayers number on structural and magnetic properties of multilayer samples was also investigated. Three samples with different number of bilayers $n$$Al_2O_3$/Pt 10 nm /(Fe 05 nm/Pt 0.3 nm)$_n$/Pt 5 nm ($n = 5$, 10, 15) were grown on columnar Pt buffer layer D. AFM measurements performed on Pt cover layer did not show any significant changes of the cover layer surface roughness for different bilayers numbers (not shown here). It may seem at odds with the observed in XRR increasing roughness of Fe/Pt interface described above, but deposition of thick (5 nm) Pt cover layer causes flattening of the film surface.

3.3. Magnetic properties of Fe/Pt multilayers deposited on columnar Pt 10 nm buffer layer (D)

$M(H)$ hysteresis loops of Al_2O_3/Pt 10 nm/(Fe 0.5 nm/ Pt 0.3 nm)$_n$/Pt 5 nm ($n = 5$, 10, 15) samples were measured by MOKE magnetometer. Influence of increasing number of bilayers is visible in Fig. 5, where magnetic parameters obtained from MOKE measurements are presented. External magnetic field was applied parallel to the sample surface (in-plane direction) or perpendicular to the sample surface (out-of-plane direction). For the magnetic field applied in-plane $M(H)$ hysteresis loops showed saturation of magnetisation for all samples. Increasing number of bilayers causes no significant changes of coercivity. Ratio of remanence to saturation magnetisation value M_r/M_s stays on the same level independently of n. Slightly different magnetic behaviour can be observed for the out-of-plane direction. Saturation of the magnetisation was not possible even at the maximum magnetic field of 20 kOe, therefore in Fig. 5 we present ratio of remanence value M_r to maximum magnetisation value $M_{\max}$ measured at the maximum applied external magnetic field. When the number of bilayers is 15, we observe significant increase of coercivity (to the value of 440 Oe) value comparing to samples with $n = 5$ or 10 which seems to be due to a superposition of hysteresis for very small amount of the phase characterized by perpendicular anisotropy (rectangular hysteresis with $H_c = 5$ kOe) and for the rest of the sample with easy-plane anisotropy ($H_c = 0$). It can be related to a formation of the region with higher Fe/Pt interface roughness

in this sample. However, only a small part of sample with $n = 15$ consists of the region with higher Fe/Pt interface roughness, so shape anisotropy still stays dominant and the hysteresis loop shows in-plane magnetisation easy axis. As it was noticed from the XRR measurements presented above, the interface roughness exceeds the nominal bilayer thickness with increasing number of bilayers, therefore it seems that occurrence of perpendicularly magnetised phase is due to the formation of the region with higher Fe/Pt interface roughness in the upper part (11th to 15th bilayer) of the sample with 15 bilayers.

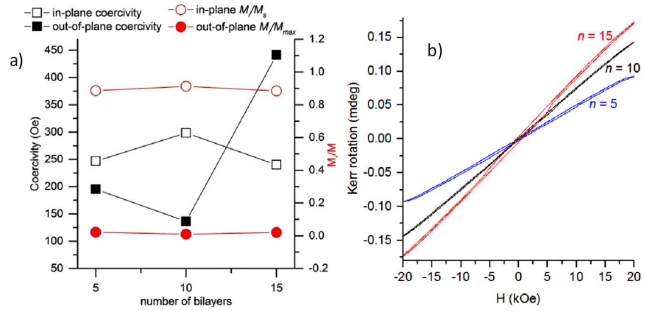

Fig. 5. (a) Coercivity and M_r/M_s (in-plane) or $M_r/M_{\max}$ (out-of-plane) values of samples Al_2O_3/Pt 10 nm/(Fe 0.5 nm/Pt 0.3 nm)$_n$/Pt 5 nm ($n = 5$, 10, 15) obtained from MOKE measurements. M_r denotes remanence value, M_s — saturation magnetisation, and $M_{\max}$ — magnetisation value measured at the maximum applied external magnetic field of 20 kOe. (b) $M(H)$ hysteresis loops for the same sample as in (a) obtained from MOKE measurements for external magnetic field applied perpendicular to the sample plane. Fe/Pt multilayers were deposited on Pt buffer layers with columnar structure. "In-plane" corresponds to external magnetic field applied parallel to the sample surface and "out-of-plane" to the field applied perpendicularly to the sample surface.

3.4. Structural properties of Fe/Pt multilayers deposited on monocrystalline 10 nm Pt (111) buffer layer (E)

Another set of Fe/Pt multilayer samples was prepared on the monocrystalline Pt buffer layer E with a configuration Al_2O_3/Pt 10 nm/(Fe 0.5 nm/Pt 0.5 nm)$_n$/Pt 10 nm, where n is a number of bilayers (5, 10, 15). *In situ* RHEED and LEED measurements were performed on all successive layers and the obtained RHEED patterns are shown in Fig. 3b in Sect. 3.2. RHEED images for all successive Fe/Pt layers were analogical to the Pt buffer layer E indicating that deposited Fe/Pt layers reproduced the crystallographic structure of the buffer layer. Also RHEED intensity oscillations were observed during subsequent Fe/Pt layers deposition proving good epitaxial growth (2D growth mode) for both Fe and Pt. Contrarily to a bulk iron with bcc structure the RHEED and LEED images confirmed fcc (111) growth of both Fe and Pt. Fcc structure of Fe on Pt is known to occur for small layer thicknesses up to 0.8÷3.4 nm depending on the author [15–17] [28].

In case of fcc-(111) Fe grown on fcc-(111) Pt in-plane misfit is 0.76% resulting in compressive strain of the first Fe layers. On each successive Fe layer of 0.5 nm in the RHEED images splitting of the outer streaks was observed (marked with arrows in Fig. 3b). Splitting of the outer streaks is probably due to the fact that incident electron beam "sees" both Fe grains formed during growth and the underneath Pt layer which is not completely covered for such small Fe layer thickness of 0.5 nm. In each streaks pair the outer ones derive from Fe and the inner ones — from Pt due to the differences in the lattice constants. Disappearance of splitting on Pt layers is caused by filling of the spaces between Fe grains during Pt layer deposition resulting in surface smoothening. Roughening and smoothening of the surface was also seen as alternating broadening (on Fe layers) and sharpening (on Pt layers) of the RHEED streaks during growth. Changes of the layer surface during deposition of Fe and Pt layers were visible also in LEED images. On each Pt layer LEED spots were dot-shaped and on each Fe layer — droplet-shaped. Change of the spots shape is caused by a presence of two materials — Fe and Pt — of different lattice constants during the measurement of the Fe layer. The same RHEED and LEED images were observed during growth of successive Fe/Pt bilayers.

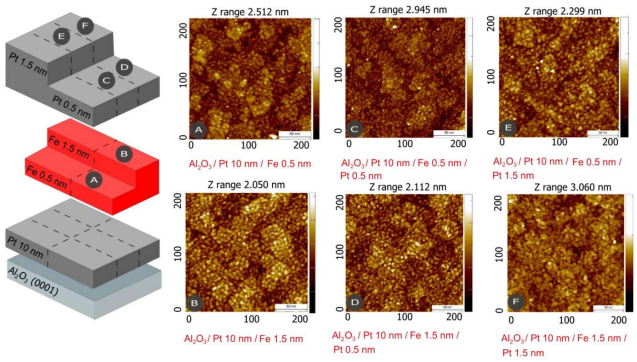

Fig. 6. STM images of successive growth steps of Fe and Pt in $Al_2O_3(0001)$/Pt 10 nm/Fe 0.5 and 1.5 nm/Pt 0.5 and 1.5 nm.

Presented interpretation of RHEED and LEED experiments was further confirmed by *in situ* STM measurements (Fig. 6). On Pt buffer layer E two Fe layers of individual thickness 0.5 nm and 15 nm were deposited as separated steps. STM measurements performed on both Fe layers proved a formation of grains that are uniformly distributed on the underneath Pt layer as shown in Fig. 6. As expected, volume of the islands increases with the increasing nominal layer thickness. Next two steps of Pt (also 0.5 nm and 15 nm thick) were deposited perpendicularly to the underneath Fe steps. STM images show smoothening of the Pt surface with increasing thickness which was also concluded from RHEED and LEED images. *In situ* STM gave us possibility to observe growth of nonoxidised Fe layers in the investigated Fe/Pt bilayers deposited at RT, which was impossible using *ex situ* AFM.

To check possible changes of the structural and magnetic properties depending on individual Fe and Pt layer thickness we have increased it from 0.5 to 1 nm and additional samples with the configuration Al_2O_3/Pt 10 nm/(Fe 1 nm/Pt 1 nm)$_n$/Pt 10 nm where n = 5, 10, 15 were grown. No changes in RHEED and LEED patterns (not shown here) were observed in comparison with analogical Al_2O_3/Pt 10 nm/(Fe 0.5 nm/Pt 0.5 nm)$_n$/Pt 10 nm series, but additional XRD experiments were performed on both sample series deposited on monocrystalline Pt buffer layers.

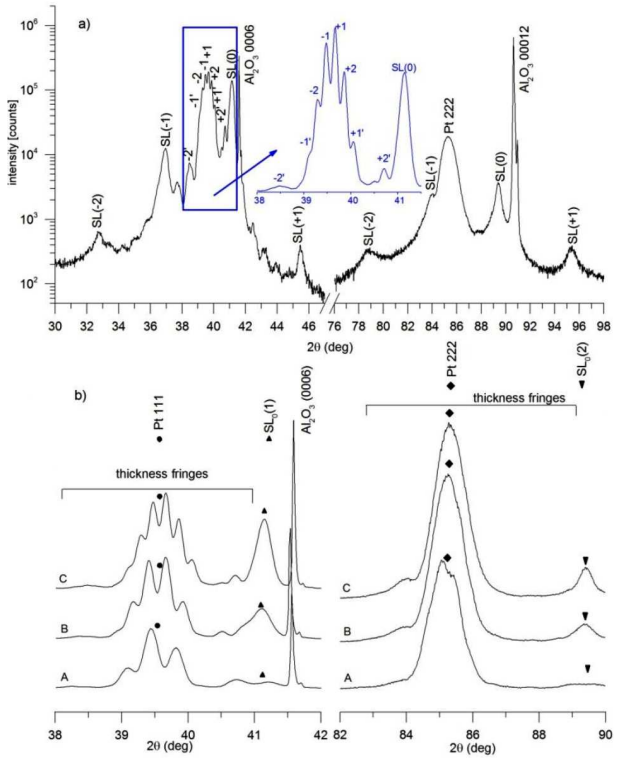

Fig. 7. $\theta-2\theta$ XRD diffraction patterns: (a) for the sample Al_2O_3/Pt 10 nm/(Fe 1 nm/Pt 1 nm)$_{15}$/Pt 10 nm. Logarithmic scale was chosen to emphasise important details of the pattern which are not visible for a linear scale. (b) Insets of XRD diffraction patterns in the vicinity of (111) and (222) Pt peaks, respectively, for Fe/Pt multilayers with different number of Fe/Pt bilayer repetitions: A — Al_2O_3/Pt 10 nm/(Fe 1 nm/Pt 1 nm)$_5$/Pt 10 nm, B — Al_2O_3/Pt 10 nm/(Fe 1 nm/Pt 1 nm)$_{10}$/Pt 10 nm, C — Al_2O_3/Pt 10 nm/(Fe 1 nm/Pt 1 nm)$_{15}$/Pt 10 nm. Positions of the characteristic lines in all patterns are indicated with symbols of different shape. Curves are shifted for better visibility.

Diffraction patterns of both sample series with X = 0.5 nm and 1 nm and for all number of bilayers repetition n, confirmed multilayers growth direction as [111]. Individual bilayer thicknesses calculated from the satellite peaks (SL 0, SL±1, SL±2) positions were in good agreement with the nominal thicknesses for both series. Well-developed Kiessig fringes present in the patterns (see Fig. 7a) originate from Pt layer thicknesses — both buffer and cover layer (lines denoted as $-2'$, $-1'$, $+1'$, and $+2'$). Lines -2, -1, $+1$, $+2$ originate from the multilayer structure and indicate presence of very sharp Fe/Pt interfaces in the multilayers.

3.5. Magnetic properties of Fe/Pt multilayers deposited on monocrystalline 10 nm Pt (111) buffer layer (E)

In the $M(H)$ measurements performed by VSM (Fig. 8a) on the sample: Al_2O_3/Pt 10 nm/(Fe 0.5 nm/Pt 0.5 nm)$_n$/Pt 10 nm, where n is a number of bilayers (5, 10, 15), the external magnetic field was applied perpendicularly to the sample surface (out-of-plane

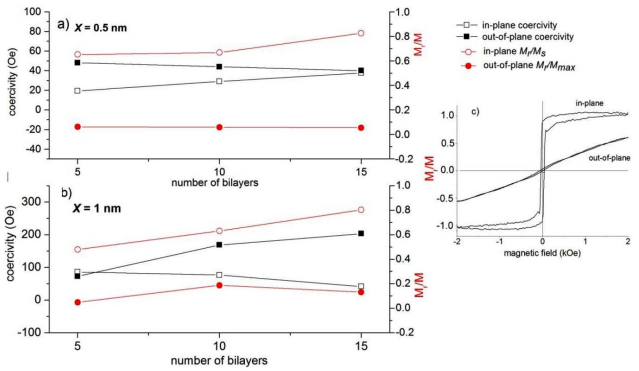

Fig. 8. Coercivity and M_r/M_s (in-plane) or $M_r/M_{\max}$ (out-of-plane) values for Fe/Pt multilayer samples with different number of bilayers (n = 5, 10 or 15) obtained from VSM measurements for Al_2O_3/Pt 10 nm/(Fe X nm/Pt X nm)$_n$/Pt 10 nm for (a) X = 0.5 nm and (b) X = 1 nm. M_r denotes remanence value, M_s — saturation magnetisation, and $M_{\max}$ — magnetisation value measured at the maximum applied external magnetic field of 2 kOe. Vertical axis description M_r/M means that M can be either M_s (for in-plane loops) or $M_{\max}$ (for out-of plane loops). Fe/Pt multilayers were deposited on monocrystalline Pt buffer layer E. "In-plane" corresponds to external magnetic field applied parallel to the sample surface and "out-of-plane" to field applied perpendicularly to the sample surface. (c) Typical magnetic hysteresis loops of the Fe/Pt multilayer sample deposited on monocrystalline Pt buffer layer. X = 1 nm, n = 15.

direction) and parallel to the sample surface (in-plane direction). The measurements revealed that all samples have easy magnetisation axis parallel to the sample plane due to dominant contribution of the shape anisotropy. For the in-plane direction we observe the slight increase of coercivity values with increasing number of bilayers as well as increase of M_r/M_s ratio. No significant changes of coercivity were observed for out-of-plane direction. In Fig. 8a for the out-of-plane direction the ratio of $M_r/M_{\max}$ ($M_{\max}$ is magnetisation value at the maximum applied external magnetic field as saturation of the magnetisation was not possible even at the maximum magnetic field of 2 kOe) is presented. As we

did not observe significant increase of coercivity values in the out-of-plane direction, we conclude that the region of higher Fe/Pt interface roughness was not formed in the sample with $X = 0.5$ nm deposited on monocrystalline buffer layer E unlike in the Fe/Pt multilayers deposited on columnar Pt buffer layer D. This result is in good agreement with structural results described so far. Additional VSM measurements of $M(H)$ hysteresis loops were performed in out-of-plane direction in the maximum applied external magnetic film of 10 kOe and still saturation of magnetisation was not possible.

$M(H)$ hysteresis loops for the samples of the configuration Al_2O_3/Pt 10 nm/(Fe 1 nm/Pt 1 nm)$_n$/Pt 10 nm where $n = 5$, 10, 15 were measured using VSM. In-plane coercivity decreased with the increasing number of bilayers. In the out-of-plane direction slight increase of the coercivity values with increase of number of multilayers was observed but still maximum measured value was over twice smaller than the value obtained for Fe/Pt multilayers deposited on Pt buffer layer D of columnar structure with $n = 15$. All samples have in-plane magnetisation easy axis due to a dominant shape anisotropy component.

4. Conclusions

The influence of Pt buffer layer structure, individual layer thickness and number of bilayers on structural and magnetic properties of (111) Fe/Pt multilayers was investigated in detail. Firstly, series of 10 nm Pt layers was deposited on Al_2O_3 using various substrate cleaning methods and deposition parameters. Monocrystalline 10 nm Pt buffer layer was possible to obtain only with deposition at 750 °C on pre-annealed substrate cleaned by method including etching in ammonia solution. As the second type of buffer layer columnar Pt film was used. Also (111) Fe/Pt multilayers deposited on the columnar Pt buffer layer were studied. Multilayers deposited on columnar Pt buffer layer revealed in-plane magnetisation easy axis due to the dominant contribution of shape anisotropy. In-plane easy magnetisation axis can be in fact expected as in (111)-oriented FePt alloys even with perfect $L1$-ordering the easy magnetization axis is tilted by 34° from the sample plane. Roughness of Fe/Pt interfaces was increasing with increase of number (up to 15) of deposited bilayers reaching the value of 0.9 nm that exceeded nominal bilayer thickness of 0.8 nm. This effect was observed both in RHEED and XRR measurements. Degradation of Fe/Pt interfaces in the upper part of the sample (11th to 15th bilayer) with 15 bilayers caused increase of coercivity value in the out-of-plane direction in comparison to the sample with 5 or 10 bilayers.

When multilayers were deposited on monocrystalline 10 nm Pt buffer layer, we observed sharp and smooth Fe/Pt interfaces regardless of the number of bilayers in RHEED and XRD experiments. Growth of all successive layers in [111] direction was confirmed in XRD experiments. Roughness of Fe/Pt interfaces was independent of the number of bilayers. This conclusion seems to be confirmed by lack of significant changes of out-of-plane coercivity values when $X = 0.5$ nm and $n = 15$. As expected, easy magnetisation axis was again parallel to sample surface. Change of individual Fe and Pt layer thickness from 0.5 to 1 nm did not cause any significant structural changes.

Magnetic properties of the Fe/Pt multilayers are influenced by the Pt buffer layer structure. Columnar structure of the buffer layer induces presence of perpendicularly magnetised phase due to degradation of the Fe/Pt interface flatness with increasing number of bilayers in the upper part of the sample. In the case of multilayers grown on the monocrystalline buffer layer no such effect is being observed. Independent of the buffer layer quality of all multilayer samples revealed in-plane easy magnetisation axis.

References

[1] A.M. Zhang, W.H. Zhu, X.S. Wu, *J. Kor. Phys. Soc.* **63**, 521 (2013).

[2] M. Jaafar, R. Sanz, J. McCord, J. Jensen, R. Schäfer, M. Vázquez, A. Asenjo, *Phys. Rev. B* **83**, 094422 (2011).

[3] T. Hasegawa, W. Pei, T. Wang, Y. Fu, T. Washiya, H. Saito, S. Ishio, *Acta Mater.* **56**, 1564 (2008).

[4] Y. Wang, P. Sharma, A. Makino, *J. Phys. Condens. Matter* **24**, 076004 (2012).

[5] Y.-N. Hsu, S. Jeong, D.E. Laughlin, D.N. Lambeth, *J. Appl. Phys.* **89**, 7068 (2001).

[6] A.S. Kamzin, F. Wei, V.R. Ganeev, A.A. Valiullin, L.D. Zaripova, *Tech. Phys.* **59**, 452 (2014).

[7] A.S. Kamzin, F. Wei, V.R. Ganeev, A.A. Valiullin, L.D. Zaripova, *Phys. Solid State* **55**, 1855 (2013).

[8] Z. Li, Y. Li, X. Liu, W. Lu, J. Bai, F. Wei, D. Wei, *IEEE Trans. Magn.* **47**, 3092 (2011).

[9] J.P. Liu, C.P. Luo, Y. Liu, D.J. Sellmyer, *Appl. Phys. Lett.* **72**, 483 (1998).

[10] J.P. Wang, Y.Y. Zou, C.H. Hee, T.C. Chong, Y.F. Zheng, *IEEE Trans. Magn.* **39**, 1930 (2003).

[11] F. Wang, X.-H. Xu, *Chin. Phys. B* **23**, 036802 (2014).

[12] Y. Endo, N. Kikuchi, O. Kitakami, Y. Shimada, *J. Appl. Phys.* **89**, 7065 (2001).

[13] H. Lassri, M. Abid, R. Krishnan, *J. Magn. Magn. Mater.* **172**, 31 (1997).

[14] C. Luo, D. Sellmyer, *IEEE Trans. Magn.* **31**, 2764 (1995).

[15] A. Fnidiki, J.S. Douheret, J. Teillet, H. Laasri, R. Krishnan, *J. Magn. Magn. Mater.* **156**, 41 (1996).

[16] M. Abid, H. Lassri, R. Krishnan, M. Nyvlt, S. Visnovsky, *J. Magn. Magn. Mater.* **214**, 99 (2000).

[17] A. Simopoulos, E. Devlin, A. Kostikas, *Phys. Rev. B* **54**, 9931 (1996).

[18] S.C. Chou, C.C. Yu, Y. Liou, Y.D. Yao, D.H. Wei, T.S. Chin, M.F. Tai, *J. Appl. Phys.* **95**, 7276 (2004).

[19] T.J. Minvielle, R.L. White, M.L. Hildner, R.J. Wilson, *Surf. Sci.* **366**, L755 (1996).

[20] O. Benamara, E. Snoeck, M. Respaud, T. Blon, *Surf. Sci.* **605**, 1906 (2011).

[21] B.M. Lairson, M.R. Visokay, R. Sinclair, S. Hagstrom, B.M. Clemens, *Appl. Phys. Lett.* **61**, 1390 (1992).

[22] H. Zhou, P. Wochner, A. Schops, T. Wagner, *J. Cryst. Growth* **234**, 561 (2002).

[23] L.P. Van, O. Kurnosikov, J. Cousty, *Surf. Sci.* **411**, 263 (1998).

[24] O. Kurnosikov, L. Pham Van, J. Cousty, *Surf. Interface Anal.* **613**, 608 (2000).

[25] P.R. Ribič, G. Bratina, *Surf. Sci.* **601**, 44 (2007).

[26] R. Verre, R.G.S. Sofin, V. Usov, K. Fleischer, D. Fox, G. Behan, H. Zhang, V. Shvets, *Surf. Sci.* **606**, 23 (2012).

[27] S. Curiotto, D. Chatain, *Surf. Sci.* **603**, 2688 (2009).

[28] M. Zhang, F. Pan, B. Liu, *J. Phys. Condens. Matter* **9**, 7623 (1997).